Role of Lewis Acids of MIL-101(Cr) in the Upgrading of Ethanol to n-Butanol

Jian Zhou[†], Yuqin Tong[†], Yaohui He, Pengxiang Tu, Bing Xue, Yunhui Cheng, Jie Cen, Yifan Zheng, Jun Ni* and Xiaonian Li

Institute of Industrial Catalysis, Zhejiang University of Technology, Hangzhou, China

The upgrading of bioethanol to n-butanol has recently been a focus of considerable attention due to the advantages of n-butanol over bioethanol as a sustainable fuel. The efficiency of this reaction is highly dependent on the development of catalysts, where understanding how catalysts perform is essential. However, traditional catalysts are normally composed of several kinds of active sites that work together synergistically in reactions, making it challenging to identify the role that individual active sites play. Herein, we synthesized three chromium-based MOFs ((MIL-101(Cr), where MIL stands for Matériaux Institut Lavoisier) with different Lewis acidities but without any basic sites. The linear relationship between Lewis acidities and their dehydration and condensation abilities suggests that there is a competition between the ethanol dehydration to diethyl ether and acetaldehyde condensation on Lewis acids. Upon the introduction of Pd, the Lewis acidity also dominates the particle size of Pd and then the dehydrogenation and hydrogenating abilities of catalysts.

Keywords: Lewis acid, MIL-101(Cr), ethanol, n-butanol, Pd catalysts

INTRODUCTION

The upgrading of bioethanol to n-butanol has recently been a focus of considerable attention from both academic and industrial fields, given the advantages of n-butanol over bioethanol as a sustainable fuel (Jiang et al., 2016; Wu et al., 2017). As shown in **Scheme 1**, this reaction generally follows the Guerbet route and consists of four steps (ethanol dehydrogenation to acetaldehyde, aldol condensation of acetaldehyde followed by dehydration to form crotonaldehyde, and two hydrogenations of crotonaldehyde to yield n-butanol), in which acetaldehyde condensation is regarded as the rate-determining step (Wu et al., 2018).

It is known that Lewis bases or Lewis acid-base pairs are active for acetaldehyde condensation. For a Lewis base-catalyzed reaction, Lewis bases abstract α-H from an acetaldehyde molecule, generating an enolate species that attacks another acetaldehyde molecule for the condensation to occur (Liang et al., 2019). However, catalysts with strong Lewis bases are prone to deactivate due to the acetaldehyde polycondensation (Ordomsky et al., 2010). For the reaction over Lewis acid-base pairs, the strength of Lewis bases has to be moderate, and Lewis acids are considered responsible for adsorbing the second acetaldehyde molecule (Sato et al., 2012). Although the ability of catalysts to remove α-H from acetaldehyde molecule is reduced, the catalysts normally outperform Lewis bases in terms of activity and stability. This highlights the importance of Lewis acids as they not only act as sites for the adsorption of acetaldehyde but also as active centers for acetaldehyde activation. This statement is difficult to verify because catalysts often contain both Lewis acid and base sites, and Lewis base can also activate acetaldehyde.

Scheme 1 | The proposed reaction network for ethanol conversion: the Guerbet reaction is in the dotted box, and the main by-products diethyl ether, ethylene, and ethyl acetate are on the periphery.
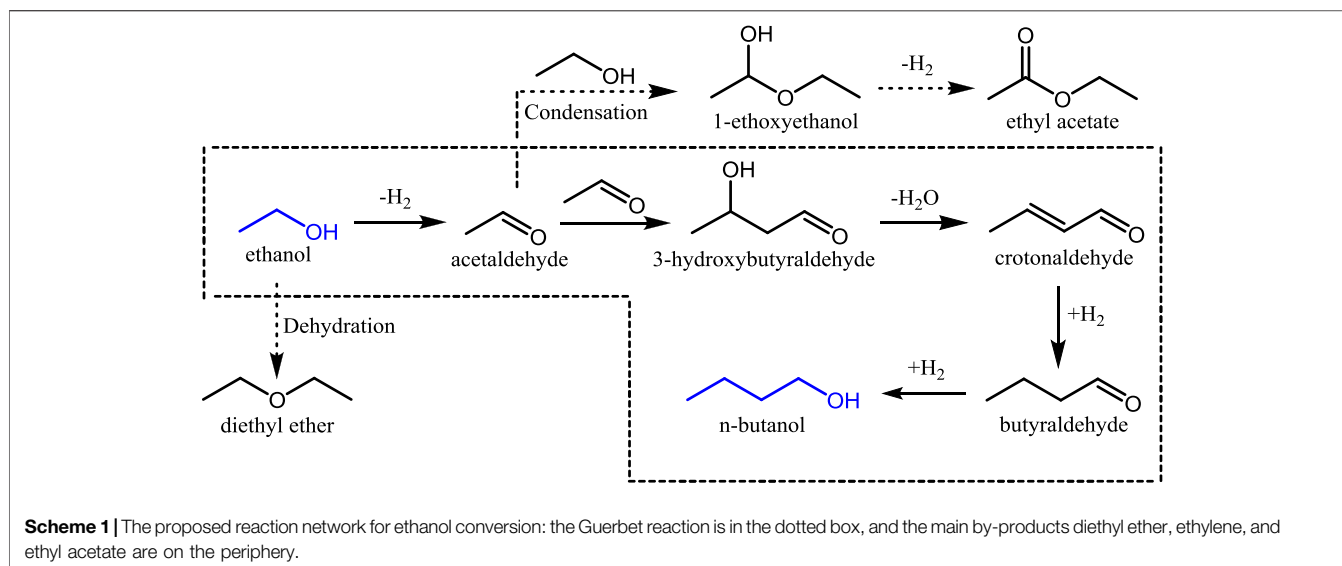
Recently, our group developed Pd@UiO-66 catalysts, in which Pd nanoparticles are favorable for ethanol dehydrogenation and crotonaldehyde hydrogenation while coordinatively unsaturated Zr sites acting as Lewis acids are very active toward the aldol condensation of acetaldehyde (Jiang et al., 2018). Because of the presence of a large number of coordinatively unsaturated Zr sites, the Pd@UiO-66 catalysts have a much lower apparent activation energy of aldol condensation than our previously reported Cu-CeO$_2$/AC catalysts (55.8 vs. 70.1 kJ·mol^{-1}). However, we still cannot totally exclude the involvement of a trace of Lewis bases of UiO-66 in this reaction.

MIL-101(Cr) was first developed by Férey and has the formula Cr$_3$X(H$_2$O)$_2$O(BDC)$_3$·nH$_2$O (where X is F or OH, BDC is terephthalic acid, and n is ~25) (Férey et al., 2005). It is made from the linkage of 1,4-BDC anions and inorganic trimmers that consist of three Cr atoms in an octahedral environment with four oxygen atoms of the bidentate dicarboxylates, one μ$_3$O atom, and one oxygen atom from the terminal water or fluorine group. After the removal of terminal water molecules or fluorine group, it has numerous potential unsaturated Cr sites (up to 3.0 mmol·g^{-1}), which can provide Lewis acid sites for catalytic reactions (Hwang et al., 2008). It also has a large pore size (ca. 2.9 and 3.4 nm) and

TABLE 1 | Catalytic performance of various Pd/MIL-101(Cr) catalysts.[a]

Catalyst	Conversion (%)	Selectivity[b] (%)							BuOH yield (%)
		AcH	Ether	EA	BuH	BuOH	C$_6$ products	Others	
Pd/MIL-101(Cr)-1	22.8	7.5	6.2	3.3	4.9	51.6	17.1	8.0	11.8
Pd/MIL-101(Cr)-2	16.6	7.1	16.5	1.8	1.6	48.0	15.0	8.2	8.0
Pd/MIL-101(Cr)-3	17.6	8.8	11.4	1.8	2.7	47.9	17.5	8.8	8.4

[a]Conversion, selectivity, and yield were obtained at steady state; reaction conditions: 0.5 g catalyst, 523 K, 2 MPa, LHSV = 2 h^{-1}, and N$_2$/ethanol(v/v) = 250:1.
[b]AcH = acetaldehyde; ether = diethyl ether; EA = ethyl acetate; BuH = butyraldehyde; BuOH = n-butanol; C$_6$ products mainly include 2-ethylbutyraldehyde, hexaldehyde, 2-ethylbutanol, and 1-hexanol; other products mainly include 2-pentanone, 1,1-diethoxyethane, and butyl acetate.

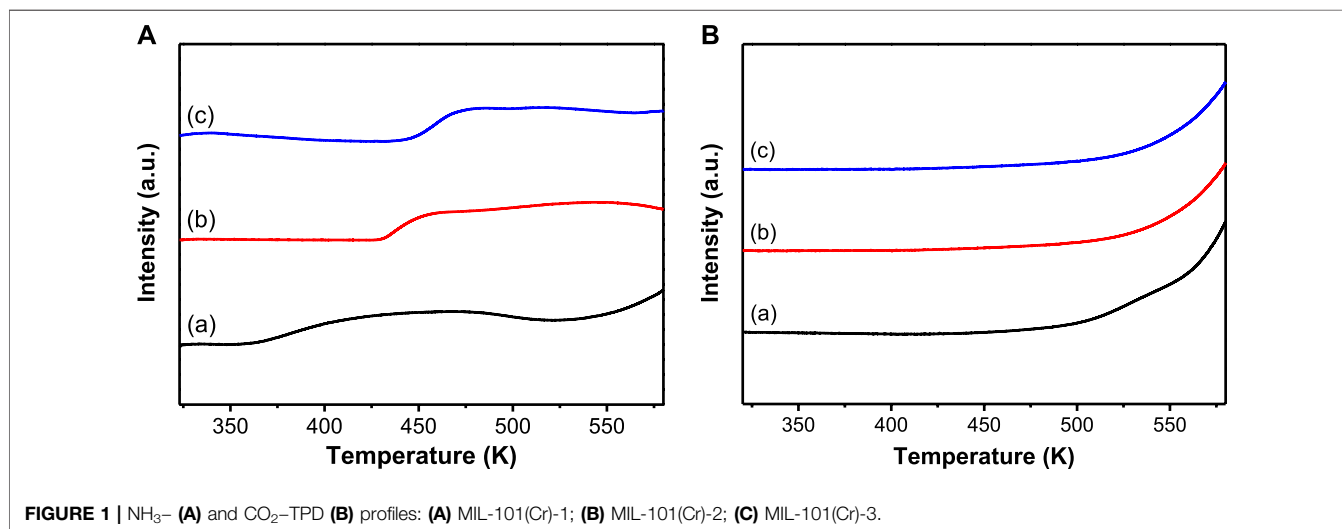**TABLE 2 |** Activity of catalysts in the key steps of the Guerbet route.

Catalyst	Activity of catalysts (%)			
	Dehydrogenation[a]	Dehydration[b]	Condensation[c]	Hydrogenation[d]
Pd/MIL-101(Cr)-1	93.8	6.2	83.0	83.0
Pd/MIL-101(Cr)-2	83.5	16.5	74.6	74.6
Pd/MIL-101(Cr)-3	88.6	11.4	78.0	78.0

[a]Dehydrogenation ability includes the selectivities of ethanol derivatives except for diethyl ether.
[b]Dehydration ability includes the selectivity of diethyl ether.
[c]Condensation ability includes the selectivities of butyraldehyde, n-butanol, C$_6$ products, and others. All of them are derived from acetaldehyde condensation.
[d]Hydrogenation ability includes the selectivities of butyraldehyde, n-butanol, C$_6$ products, and others.
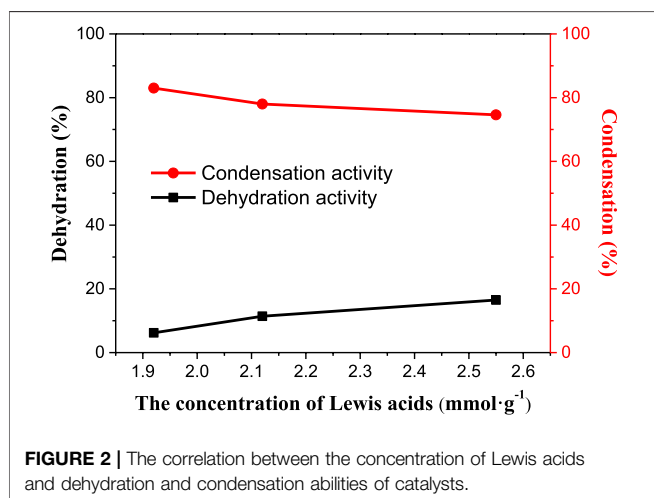
FIGURE 1 | NH_3- **(A)** and CO_2-TPD **(B)** profiles: **(A)** MIL-101(Cr)-1; **(B)** MIL-101(Cr)-2; **(C)** MIL-101(Cr)-3.

large surface area (ca. 4,000 $m^2 \cdot g^{-1}$), which are desirable for depositing small Pd NPs (Pan et al., 2010). Therefore, we employed MIL-101(Cr) as support for the preparation of Pd/MIL-101(Cr) catalysts and investigated how Lewis acid affects the conversion of ethanol to n-butanol. In order to vary the concentration and strength of unsaturated Cr sites, three MIL-101(Cr) supports were synthesized hydrothermally using the following: 1) $Cr(NO_3)_3 \cdot 9H_2O$ without HF, 2) $CrCl_3 \cdot 6H_2O$ without HF, and 3) $Cr(NO_3)_3 \cdot 9H_2O$ with HF, which were then designated as MIL-101(Cr)-1, MIL-101(Cr)-2, and MIL-101(Cr)-3, respectively. After loading Pd, they were named as Pd/MIL-101(Cr)-1, Pd/MIL-101(Cr)-2, and Pd/MIL-101(Cr)-3.

The catalytic performance of three Pd/MIL-101(Cr) catalysts was first evaluated, as shown in **Table 1**. Pd/MIL-101(Cr)-1 displays the highest ethanol conversion (22.8%) and selectivity of n-butanol (51.6%), whereas Pd/MIL-101(Cr)-2 and Pd/MIL-101(Cr)-3 give lower ethanol conversions and n-butanol selectivities, but higher selectivities of diethyl ether. The formation of diethyl ether can be directly linked to the presence

of Brønsted or Lewis acids over catalysts (Xin et al., 2014; Krutpijit et al., 2020). However, the activity of acetaldehyde condensation cannot be associated with a single product because, in this tandem ethanol conversion reaction, the product of acetaldehyde condensation (crotonaldehyde) will be further transformed into butyraldehyde, n-butanol, C_6 products, and others. Thus, the catalytic performance of catalysts was reanalyzed and presented in **Table 2** in terms of the activity of dehydrogenation, dehydration, condensation, and hydrogenation of catalysts. Pd/MIL-101(Cr)-1 also exhibits the highest dehydrogenation, condensation, and hydrogenation activities but the lowest dehydration activity.

In order to understand the catalytic behavior of catalysts, three MIL-101(Cr) supports and Pd/MIL-101(Cr) catalysts were then characterized. All MIL-101(Cr) supports show well-crystallized morphology and similar grain size in SEM (**Supplementary Figure S1**). The N_2 adsorption-desorption over the MIL-101(Cr) supports also indicates that they have a similar surface area, pore volume, and average pore diameter, as shown in **Supplementary Table S1**. These similarities of morphology and textural properties ensure that a similar dispersion of Pd metals can be achieved, given the same incipient wetness impregnation method is applied.

Then, the thermal stability of MIL-101(Cr) supports was carried out and three weight-loss steps of MIL-101(Cr) supports were observed (**Supplementary Figure S2**). In the temperature range of 323–473 K, the weight loss can be ascribed to the release of free and bound water molecules (Wang et al., 2019). MIL-101(Cr)-2 gave the highest weight loss, followed by MIL-101(Cr)-3 and then MIL-101(Cr)-1. The removal of hydroxylic or fluorine groups takes place in the temperature range of 473–623 K. And further higher temperature (>623 K) gives rise to the decomposition of MIL-101(Cr) supports (the degradation of dicarboxylate linkers), as indicated by the appearance of COO signal detected by mass spectrometry, and results in the formation of Cr_2O_3. Since the catalyst evaluation occurs at 523 K, 100 K lower than the decomposition temperature (623 K), the catalysts are stable during the reaction.
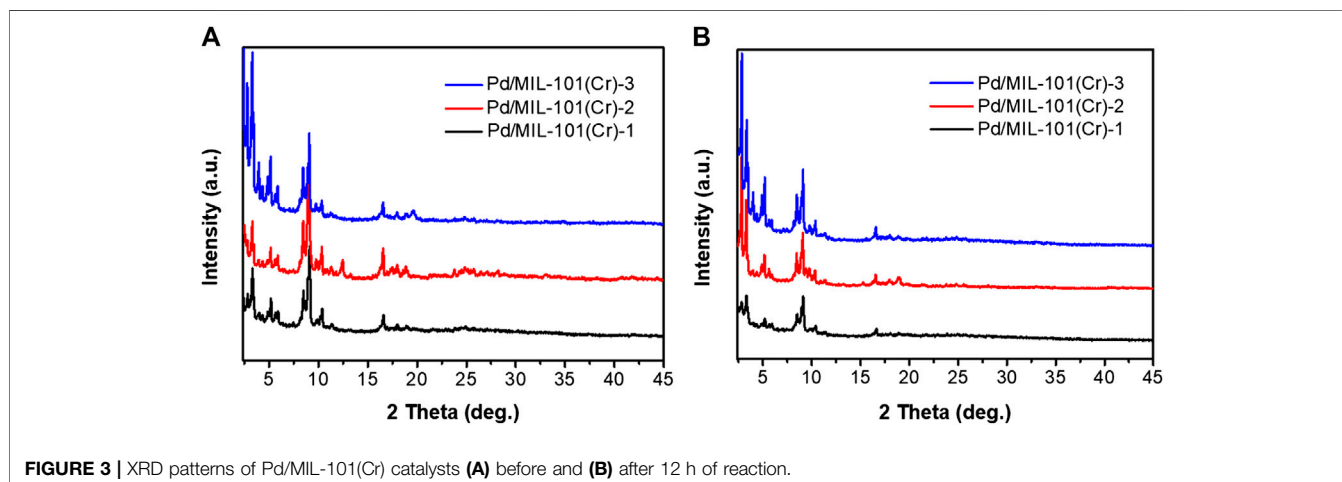

FIGURE 2 | The correlation between the concentration of Lewis acids and dehydration and condensation abilities of catalysts.

FIGURE 3 | XRD patterns of Pd/MIL-101(Cr) catalysts **(A)** before and **(B)** after 12 h of reaction.

The thermal analysis also suggests that the unsaturation of Cr sites may vary depending on the preparation method of the MIL-101(Cr) supports because the higher the amounts of water molecules and hydroxylic or fluorine groups are removed, the higher the amount of unsaturated Cr sites will be. In this case, the Lewis acidity of catalysts will change accordingly. Thus, NH_3–TPD was performed to measure the acidity of catalysts, as illustrated in **Figure 1A**.

All MIL-101(Cr) supports exhibit a single and broad peak in the temperature range of 350–523 K (**Figure 1A**) due to the NH_3 desorption from Lewis acids (unsaturated Cr sites) (Liu et al., 2017). According to the thermal analysis, MIL-101(Cr)-1 has the lowest weight loss in that temperature range; thus, it has the lowest amount of NH_3 desorbed (1.92 mmol·g^{-1}) and weakest Lewis acidity. For the same reason, MIL-101(Cr)-2 has the highest amount of NH_3 desorbed (2.55 mmol·g^{-1}) and the strength of Lewis acids is higher than that of MIL-10(Cr)-1 (Kim et al., 2013). In the case of MIL-101(Cr)-3, the weight loss and the amount of NH_3 desorbed (2.12 mmol·g^{-1}) are

between those of MIL-101(Cr)-1 and MIL-101(Cr)-2, but the unsaturated Cr sites are coordinated with the fluorine group (Ji et al., 2018), which makes the strength of Lewis acids strongest.

As we mentioned above, the presence of base may interfere with concluding how Lewis acids influence the upgrading of ethanol to n-butanol. The basicity was then measured by CO_2–TPD, as shown in **Figure 1B**. None of the CO_2 desorption peaks was detected over all MIL-101 (Cr) supports, indicating that there are no basic sites and the MIL-101(Cr) supports only possess Lewis acid sites, which is in good agreement with the literature (Pan et al., 2010; Zhou et al., 2016). Thus, the catalytic activity can be directly correlated to the properties of Lewis acids.

We then correlated the concentration of Lewis acids to their dehydration and condensation abilities. A linear relationship is observed in **Figure 2**. With the increase in the concentration of Lewis acids, the condensation activity decreases, whereas the dehydration activity increases. The sum of dehydration and condensation abilities over different Pd/MIL-101(Cr) catalysts is almost the same (~90%); thus, the decrease of the condensation activity is directly related to the increase of the dehydration activity. Actually, it is reasonable to consider that Lewis acids may act as sites for activating both acetaldehyde and ethoxy after ethanol dehydrogenation. The self-coupling of acetaldehyde forms crotonaldehyde that is the precursor for n-butanol, whereas the self-coupling of adsorbed ethoxy gives rise to diethyl ether. The competitive adsorption between acetaldehyde and ethoxy yields the opposite relationship with the concentration of Lewis acids.

Previously, our study on Pd@UiO-66 revealed that the nature of Pd dominates the abilities of ethanol dehydrogenation and crotonaldehyde hydrogenation, being the smaller the particle size of Pd metals, the better the performance (Jiang et al., 2018). Thus, the textural properties of Pd metals in Pd/MIL-101(Cr) catalysts were analyzed. As shown in **Supplementary Table S1**, the surface area, pore volume, and average pore diameter of catalysts decrease after loading Pd on MIL-101(Cr) supports, indicating the incorporation of Pd metals in the pores of MIL-101(Cr) supports. These incorporated Pd metals do not
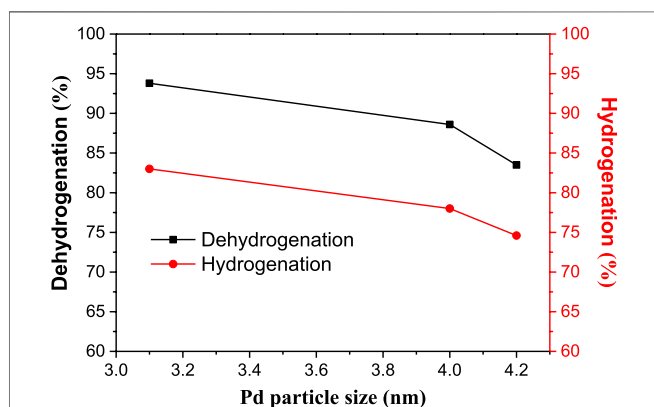

FIGURE 4 | The correlation between the Pd particle size and dehydrogenation and hydrogenation abilities of catalysts.

give any characteristic peaks in XRD patterns (**Figure 3A**) because of either their low loading (1 wt%) or small particle size. Then, we employed TEM and found that the average Pd particle size is in the range of 3.1–4.2 nm (**Supplementary Figure S3**; **Table S1**). Thus, the absence of characteristic peaks is ascribed to the low loading of Pd metals.

Pd/MIL-101(Cr)-1 has the smallest particle size of Pd (3.1 nm). It is supposed that the interaction between the support surface and the precious metals precursors is affected by parameters such as the point of zero charge (PZC) of the support, the pH of the aqueous solution, and the nature of the metallic complex (Zhu et al., 2012). In the process of synthesizing Pd/MIL-101(Cr) catalysts, the pH of PdCl$_2$ aqueous solution is ~3 and Pd exists as PdCl$_4^{2-}$ complex (Wang et al., 2010). On the other hand, assuming the Cr sites of MIL-101(Cr) supports are analogous to Cr$_2$O$_3$ with a PZC of 5.8, the surface of Cr sites is positively charged in the impregnation solution of PdCl$_2$ and may interact with the negatively charged PdCl$_4^{2-}$ complex via electrostatic attraction. In addition, ligand-exchange reactions between PdCl$_4^{2-}$ in the solution and OH$^-$ groups on the surface of supports may also result in the interaction between Pd species and the supports (Monteiro et al., 2001). In this way, MIL-101(Cr)-1 has the highest amount of Cr-O/OH sites (due to the lowest weight loss of water molecules and hydroxylic or fluorine groups); thus, the interaction between Pd complex and the support seems to be the strongest. The migration of Pd complex in the processes of drying, calcination, and reduction can be minimized; thus, the resultant catalyst Pd/MIL-101(Cr)-1 affords the highest Pd dispersion and the smallest Pd metals.

The Pd particle size was then correlated with the dehydrogenation and hydrogenating abilities of catalysts (**Figure 4**). Apparently, the increase in the particle size of Pd decreases both the dehydrogenation and hydrogenating abilities of catalysts, which is in line with our previous study. Pd/MIL-101(Cr)-1 has the smallest Pd particle size and, thus, has the highest dehydrogenation and hydrogenating abilities. Moreover, Pd/MIL-101(Cr)-1 also has the lowest concentration of Lewis acids; thus, it has the highest n-butanol yield, as shown in **Table 1**. These Pd/MIL-101(Cr) catalysts after 12 h of reaction were then examined by XRD (**Figure 3B**), and it was found that they remain intact and stable during the reaction, which is consistent with the thermal analysis above.

REFERENCES

Férey, G., Mellot-Draznieks, C., Serre, C., Millange, F., Dutour, J., Surblé, S., et al. (2005). A chromium terephthalate-based solid with unusually large pore volumes and surface area. *Science* 309, 2040–2042. doi:10.1126/science.310.5751.1119

Hwang, Y. K., Hong, D.-Y., Chang, J.-S., Jhung, S. H., Seo, Y.-K., Kim, J., et al. (2008). Amine grafting on coordinatively unsaturated metal centers of MOFs: consequences for catalysis and metal encapsulation. *Angew. Chem. Int. Ed.* 47, 4144–4148. doi:10.1002/ange.200705998

Ji, P., Drake, T., Murakami, A., Oliveres, P., Skone, J. H., and Lin, W. (2018). Tuning Lewis acidity of metal-organic frameworks via perfluorination of bridging ligands: spectroscopic, theoretical, and

In summary, three MIL-101(Cr) with different Lewis acidities can be prepared using appropriate precursors. They do not have any basic sites and thus allow us to exclusively correlate the concentration of Lewis acids to their dehydration and condensation abilities. Their linear relationship suggests that acetaldehyde coupling and ethoxy coupling occur competitively on Lewis acids. Upon the introduction of Pd, the degree of unsaturation of Cr sites dominates the particle size of Pd and, as a result, also the dehydrogenation and hydrogenating abilities of catalysts. Pd/MIL-101(Cr)-1 has the smallest Pd particle size and the lowest concentration of Lewis acids and thus has the highest n-butanol yield.

DATA AVAILABILITY STATEMENT

The original contributions presented in the study are included in the article/**Supplementary Material**; further inquiries can be directed to the corresponding author.

AUTHOR CONTRIBUTIONS

All authors listed have made a substantial, direct, and intellectual contribution to the work and approved it for publication.

FUNDING

SUPPLEMENTARY MATERIAL

The Supplementary Material for this article can be found online at: https://www.frontiersin.org/articles/10.3389/fceng.2020.586142/full#supplementary-material.

catalytic studies. *J. Am. Chem. Soc.* 140, 10553–10561. doi:10.1021/jacs.8b05765

Jiang, D., Fang, G., Tong, Y., Wu, X., Wang, Y., Hong, D., et al. (2018). Multifunctional Pd@UiO-66 catalysts for continuous catalytic upgrading of ethanol to n-butanol. *ACS Catal.* 8, 11973–11978. doi:10.1021/acscatal.8b04014

Jiang, D., Wu, X., Mao, J., Ni, J., and Li, X. (2016). Continuous catalytic upgrading of ethanol to n-butanol over Cu-CeO$_2$/AC catalysts. *Chem. Commun.* 52, 13749–13752. doi:10.1039/C6CC05860D

Kim, J., Kim, S.-N., Jang, H.-G., Seo, G., and Ahn, W.-S. (2013). CO$_2$ cycloaddition of styrene oxide over MOF catalysts. *Appl. Catal., A* 453, 175–180. doi:10.1016/j.apcata.2012.12.018

Krutpijit, C., Tochaeng, P., and Jongsomjit, B. (2020). Temperature and ethanol concentration effects on catalytic ethanol dehydration behaviors over alumina-

spherical silica particle composite catalysts. *Catal. Commun.* 145, 106102. doi:10.1016/j.catcom.2020.106102

Liang, Z., Jiang, D., Fang, G., Leng, W., Tu, P., Tong, Y., et al. (2019). Catalytic enhancement of aldol condensation by oxygen vacancy on CeO2 catalysts. *ChemistrySelect* 4, 4364–4370. doi:10.1002/slct.201900712

Liu, Y., Yang, X., Liu, H., Ye, Y., and Wei, Z. (2017). Nitrogen-doped mesoporous carbon supported Pt nanoparticles as a highly efficient catalyst for decarboxylation of saturated and unsaturated fatty acids to alkanes. *Appl. Catal., B* 218, 679–689. doi:10.1016/j.apcatb.2017.06.065

Monteiro, R. S., Dieguez, L. d. C., and Schmal, M. (2001). The role of Pd precursors in the oxidation of carbon monoxide over Pd/Al2O3 and Pd/CeO2/Al2O3 catalysts. *Catal. Today* 65, 77–89. doi:10.1016/S0920-5861(00)00547-2

Ordomsky, V. V., Sushkevich, V. L., and Ivanova, I. I. (2010). Study of acetaldehyde condensation chemistry over magnesia and zirconia supported on silica. *J. Mol. Catal. Chem.* 333, 85–93. doi:10.1016/j.molcata.2010.10.001

Pan, Y., Yuan, B., Li, Y., and He, D. (2010). Multifunctional catalysis by Pd@MIL-101: one-step synthesis of methyl isobutyl ketone over palladium nanoparticles deposited on a metal–organic framework. *Chem. Commun.* 46, 2280–2282. doi:10.1039/b922061e

Sato, A. G., Volanti, D. P., de Freitas, I. C., Longo, E., and Bueno, J. M. C. (2012). Site-selective ethanol conversion over supported copper catalysts. *Catal. Commun.* 26, 122–126. doi:10.1016/j.catcom.2012.05.008

Wang, F., Jiang, J., Wang, K., Zhai, Q., Long, F., Liu, P., et al. (2019). Hydrotreatment of lipid model for diesel-like alkane using nitrogen-doped mesoporous carbon-supported molybdenum carbide. *Appl. Catal., B* 242, 150–160. doi:10.1016/j.apcatb.2018.09.077

Wang, L., Xu, S., Chu, W., and Yang, W. (2010). Effect of Pd loading and precursor on the catalytic performance of Pd/WO3–ZrO2 catalysts for selective oxidation of ethylene. *Catal. Today* 149, 163–166. doi:10.1016/j.cattod.2009.02.041

Wu, X., Fang, G., Liang, Z., Leng, W., Xu, K., Jiang, D., et al. (2017). Catalytic upgrading of ethanol to n-butanol over M-CeO2/AC (M = Cu, Fe, Co, Ni and Pd) catalysts. *Catal. Commun.* 100, 15–18. doi:10.1016/j.catcom.2017.06.016

Wu, X., Fang, G., Tong, Y., Jiang, D., Liang, Z., Leng, W., et al. (2018). Catalytic upgrading of ethanol to n-butanol: progress in catalyst development. *ChemSusChem* 11, 71–85. doi:10.1002/cssc.201701590

Xin, H., Li, X., Fang, Y., Yi, X., Hu, W., Chu, Y., et al. (2014). Catalytic dehydration of ethanol over post-treated ZSM-5 zeolites. *J. Catal.* 312, 204–215. doi:10.1016/j.jcat.2014.02.003

Zhou, Z., Mei, L., Ma, C., Xu, F., Xiao, J., Xia, Q., et al. (2016). A novel bimetallic MIL-101(Cr, Mg) with high CO2 adsorption capacity and CO2/N2 selectivity. *Chem. Eng. Sci.* 147, 109–117. doi:10.1016/j.ces.2016.03.035

Zhu, Z., Lu, G., Guo, Y., Guo, Y., Zhang, Z., and Wang, Y. (2012). Influences of Pd precursors and preparation method on the catalytic performances of Pd-only close-coupled catalysts. *J. Ind. Eng. Chem.* 18, 2135–2140. doi:10.1016/j.jiec.2012.06.008